*Supported by the NSF.

†Research supported in part by the U. S. Air Force Office of Scientific Research.

[1]K. J. Button, C. G. Fonstad, and W. Dreybrodt, Bull. Am. Phys. Soc. 16, 417 (1971).

[2]C. G. Fonstad and R. H. Rediker, J. Appl. Phys. 42, 2911 (1971); Bull. Am. Phys. Soc. 15, 316 (1970).

[3]K. J. Button, *Solid State Resonance Spectroscopy at Submillimeter Wavelengths* in *Optical Properties of Solids*, edited by E. D. Haidemenakis (Gordon and Breach, New York, 1970), pp. 253–279; Laser Focus, 7, No. 8, 29 (1971).

[4]M. Nagasawa and S. Shionoya, J. Phys. Soc. Japan 20, 1093 (1965).

[5]J. A. Marley and R. C. Dockerty, Phys. Rev. 140, A304 (1965).

[6]D. F. Morgan and D. A. Wright, Brit. J. Appl. Phys. 17, 337 (1966).

[7]R. Summitt and N. F. Borrelli, J. Phys. Chem. Solids 26, 921 (1965). We have corrected their calculation for the correct dielectric constant, i.e., an average ϵ =12 rather than 24.

[8]D. F. Crabtree, R. N. S. M. Mehdi, and D. A. Wright, Brit. J. Appl. Phys. 2, 1503 (1969).

[9]K. J. Button, B. Lax, and D. R. Cohn, Phys. Rev. Letters 24, 375 (1970).

[10]J. Waldman, D. M. Larsen, P. E. Tannenwald, C. C. Bradley, D. R. Cohn, and B. Lax, Phys. Rev. Letters 23, 1033 (1969).

[11]K. J. Button and B. Lax, Bull. Am. Phys. Soc. 15, 365 (1970).

[12]M. Nagasawa and S. Shionoya, J. Phys. Soc. Japan 30, 158 (1971).

[13]C. G. Fonstad, A. Linz, and R. H. Rediker, J. Electrochem. Soc. 116, 1269 (1969).

[14]C. Kittel, *Introduction to Solid State Physics*, 3rd ed. (Wiley, New York, 1966), p. 321.

[15]R. Summitt, J. Appl. Phys. 39, 3762 (1968); H. J. van Daal, *ibid.* 39, 4467 (1968).

Phonons, Polaritons, and Oblique Phonons in LiIO₃ by Raman Scattering and Infrared Reflection*

W. Otaguro, E. Wiener-Avnear,† C. A. Arguello,‡ and S. P. S. Porto

*Departments of Physics and Electrical Engineering,
University of Southern California, Los Angeles, California 90007*

(Received 6 July 1971)

A detailed Raman-scattering investigation of LiIO₃, combined with the polarized infrared-reflectivity measurements, is reported. The dielectric constants determined by the Lyddane-Sachs-Teller (LST) relation (ϵ_{xx}=6.7, ϵ_{zz}=6.1) do not reveal any large contribution by the lattice dynamics to the low-frequency dielectric response. The high-temperature study of the TO Raman modes (till 220 °C) does not show any mode "softening," which could explain the critical dielectric behavior observed at very low frequencies. The study of the A-symmetry polariton curves has reconfirmed the LST dielectric values. The angular dispersion of the two upper oblique phonons of the A and E_1 symmetry is compared with theory. The intensity dependence of these oblique phonons enables the determination of the second-harmonic-generation coefficient d_{13} and the linear electro-optic coefficient r_{13} in LiIO₃. These values are compared with other published data.
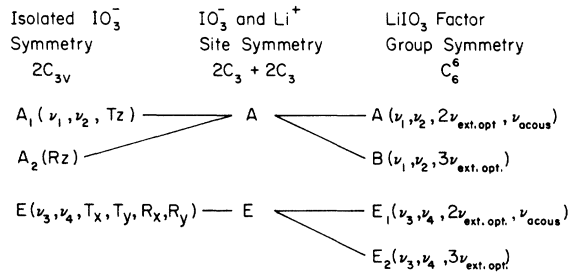
INTRODUCTION

There has been much interest lately in iodates as new nonlinear optic materials. Of this group LiIO₃ is of special interest since its nonlinear coefficients are comparable with the second harmonic nonlinear coefficient d_{13} of LiNbO₃, and the second harmonic generation (SHG) is phase matchable.[1] Several investigations into the crystal properties of LiIO₃ have resulted in contrasting reports,[1-4] and as yet an unexplained dielectric behavior.[5]

The dielectric constant along the z axis exhibits an unusual temperature and frequency behavior. As the temperature is increased from 21.5 to 256 °C (where presumably a destructive phase transition occurs), the ϵ_{zz} measured at 1000 Hz increases from 554 to values higher than 30 000, whereas the $\epsilon_{xx} = \epsilon_{yy}$ is almost temperature insensitive.[1] As a function of frequency at room temperature, ϵ_{zz} decreases from a value of 554 at 1000 Hz to approximately 6 at 3 MHz.[5] Pyroelectricity has been observed in LiIO₃; however, attempts to observe electric polarization switching with fields up to 6 kV/cm were unsuccessful.[1]

The following paper describes a detailed investigation of the Raman scattering at various temperatures combined with the polarized infrared reflectivity of LiIO₃. These studies provide information on the structural makeup of the crystal as determined from the selection rules. Also, the phonon contribution to the abnormal dielectric-constant behavior is determined from the generalized Lyddane-Sachs-Teller (LST) relation. As the lowest polariton dispersion curve also depends on the static dielectric constant, an effort was made to follow the polariton dispersion in LiIO₃ at room

Isolated IO_3^- IO_3^- and Li^+ $LiIO_3$ Factor
Symmetry   Site Symmetry   Group Symmetry
$2C_{3v}$ $2C_3 + 2C_3$ C_6^6

$A_1(\nu_1,\nu_2, T_z)$ ——— A ——— $A(\nu_1,\nu_2,2\nu_{ext.opt}, \nu_{acous})$

$A_2(R_z)$ ——— B $(\nu_1,\nu_2,3\nu_{ext.opt.})$

$E(\nu_3,\nu_4,T_x,T_y,R_x,R_y)$ —— E ——— $E_1(\nu_3,\nu_4,2\nu_{ext.opt.}, \nu_{acous})$

$E_2(\nu_3,\nu_4,3\nu_{ext.opt.})$

FIG. 1. Correlation table for $LiIO_3$.

temperature. Another interesting problem is the dispersion of the oblique phonons in $LiIO_3$.[6,7] The frequencies and intensities of the upper A and E_1 oblique phonons have been measured and compared with a general theory developed lately.[8] The oblique phonon's intensity measurements provide a new experimental method[7] for determining the nonlinear coefficients of the crystal. The SHG coefficient d_{13} and the linear electro-optic coefficient r_{13} of $LiIO_3$ are compared with the experimental values[1,9-11] obtained by different methods.

THEORY

During the present work on $LiIO_3$, the hexagonal space group C_6^6 as determined by Rosenzweig and Morosin's x-ray reinvestigation of $LiIO_3$[3] will be followed. The latter's technique and samples were much superior to those reported in earlier studies,[4] and are also completely justified by the Raman and infrared selection-rule predictions. Previous Raman spectra of iodate radicals in several solutions[12] revealed only frequencies higher than 300 cm^{-1}, which are above the lattice modes in the $LiIO_3$ crystal. It is therefore convenient to separate the vibrational problem into the following two frequency regions: (i) the iodate-ion internal modes (300–900 cm^{-1}); (ii) the lattice external modes (< 300 cm^{-1}), which include the librational and translational modes. Considering first the internal modes, the 12 degrees of freedom of the C_{3v} isolated iodate ion are divided by group theory into $3A_1 + 1A_2 + 4E$ irreducible representations; the three modes belonging to the A_1 representation consist of ν_1 (~779 cm^{-1}) and ν_2 (~390 cm^{-1}) characteristic vibrations and a translation along the z direction; the mode of the A_2 symmetry is a rotation about the z axis; and the four modes of the E symmetry consist of a degenerate translation and rotation, with respective ν_3 (~826 cm^{-1}) and ν_4 (~330 cm^{-1}) characteristic vibrations.

Both the iodate and lithium ions occupy C_3 sites in the hexagonal $LiIO_3$ lattice. The correlation diagram in Fig. 1 maps out both the site-group and the factor-group splittings, which are expected in the C_6^6 space group, with two molecules per primi-

tive cell.

On the basis of this analysis, the total of 30 degrees of freedom in $LiIO_3$ is represented by $5A + 5B + 5E_1 + 5E_2$ irreducible species. The acoustic phonons belong to the A and E_1 representations. The optical lattice modes in the external region are $2A + 3B + 2E_1 + 3E_2$. The modes of the A and E_1 symmetry are both Raman infrared active, the modes of the B representation are silent, namely, Raman and infrared inactive, and the modes of the E_2 representation are only Raman active but infrared inactive.

The Raman polarizability tensors associated with the different phonons are

$$A(z) = \begin{bmatrix} a & 0 & 0 \\ 0 & a & 0 \\ 0 & 0 & b \end{bmatrix}, \qquad E_1(x) = \begin{bmatrix} 0 & 0 & c \\ 0 & 0 & d \\ c & d & 0 \end{bmatrix},$$

$$E_1(y) = \begin{bmatrix} 0 & 0 & -d \\ 0 & 0 & c \\ -d & c & 0 \end{bmatrix}, \qquad E_2 = \begin{bmatrix} e & f & 0 \\ f & -e & 0 \\ 0 & 0 & 0 \end{bmatrix},$$

$$E_2 = \begin{bmatrix} f & -e & 0 \\ -e & -f & 0 \\ 0 & 0 & 0 \end{bmatrix}.$$

Owing to the electric polarizations of the modes of the $A(z)$ and $E_1(x, y)$ representations (indicated in the parentheses), these modes may interact with infrared radiation through absorption and reflection. The infrared reflectivity R is given by

$$R_k(\omega) = \left| \frac{[\epsilon_k(\omega)]^{1/2} - 1}{[\epsilon_k(\omega)]^{1/2} + 1} \right|^2 , \tag{1}$$

where $\epsilon_k(\omega)$ is the frequency-dependent dielectric constant along the k axis, which is related to the index of refraction n_k and the extinction coefficient δ_k by

$$\epsilon_k(\omega) = (n_k - i\delta_k)^2 . \tag{2}$$

The infrared reflectivity is related to the Raman-scattering results through the expression

$$\epsilon_k(\omega) = \epsilon_{k\infty} + \sum_j \frac{S_{kj}\omega_{kj}^2}{\omega_{kj}^2 - \omega^2 + i\Gamma_{kj}\omega} , \tag{3}$$

where $\epsilon_{k\infty}$ is the high-frequency dielectric constant, S_{kj} is the dielectric transition strength, ω_{kj} is the transverse phonon frequency, and Γ_{kj} is the damping term. In the infrared reflectivity experiments both the transverse-optic (TO) and longitudinal-optic (LO) values may be determined from the inflection points in the spectrum.[13] In the Raman experiments, the TO and LO phonons can sometimes be separated as discrete lines when applying different scattering geometries.

Neglecting damping, the phonon contribution to the low-frequency dielectric constant ϵ_k(LST) can

be rewritten from Eq. (3) as follows:

$$\epsilon_k(\text{LST})/\epsilon_k(\infty) = \prod_j \left(\omega_{kj}(\text{LO})/\omega_{kj}\right)^2 . \tag{4}$$

The dependence of $\epsilon_k(\text{LST})$ calculated from Eq. (4) as a function of temperature would therefore indicate the contribution of the phonons to the dielectric anomaly.[1] In such a case, a soft mode already verified in many displacive ferroelectrics near the ferroelectric phase transition[14,15] might be expected.

Mixed electromagnetic-mechanical excitations known as polaritons can be observed in Raman-forward-scattering experiments.[16,17] In such events the transverse-optical polarized phonons interact strongly with the electromagnetic waves whenever their energies and momentum vectors are conserved. The polariton dispersion curves can be calculated, once all the TO and LO frequencies are known, from the following relationship[17]:

$$\frac{q_k^2 c^2}{\omega^2} = \epsilon_k(\infty) + \sum_{j=1}^{N} \frac{S_{kj}\omega_{kj}^2}{\omega_{kj}^2 - \omega^2 + i\Gamma_{kj}\omega} , \tag{5}$$

where q_k is the transverse-photon momentum transfer in the Raman-scattering process. The slope of the lowest polariton curve is proportional to $[\epsilon_k(\text{LST})]^{-1/2}$,[18] and thus gives another measure of the optical-phonon contribution to the low-frequency dielectric constant.

It is well known that phonons which are both infrared and Raman active have frequencies and polarizations which are dependent on their propagation directions. Such oblique phonons have been observed in simple uniaxial crystals[19] and lately in biaxial orthorhombic NaNO_2.[8] When the electrostatic approximation holds, the general formula for the three-dimensional oblique-phonon dispersion curves were worked out.[8] Restricting the oblique-phonon propagation to a major plane, denoted as xz to relate to the experiments on LiIO_3 described later, the explicit expression for the angular dispersion is

$$\tan^2\varphi = -\frac{\epsilon_{\infty z}}{\epsilon_{\infty x}} \prod_{i=1}^{N_x} \prod_{j=1}^{N_z} \frac{(\omega_{iA}^2 - \omega_\varphi^2)[\omega_{jE}^2(\text{LO}) - \omega_\varphi^2]}{(\omega_{jE}^2 - \omega_\varphi^2)[\omega_{iA}^2(\text{LO}) - \omega_\varphi^2]} , \tag{6}$$

where φ is the angle between the oblique-phonon propagation in the xz plane and the z axis. The frequencies ω_{iA} and ω_{jE} are of the fundamental transverse modes which are polarized along the z and x axes, respectively. The Raman-scattering efficiency of the TO mode is due to the electron-lattice interaction $\alpha_{ijk}^m S_k^{m1/2}$, whereas that of the LO mode contains an additional pure electronic term ξ_{ijk}, which is equal to four times the SHG term, d_{ijk}. These contributions to the Raman cross section are related[20] to the linear electro-optic effect r_{ijk}:

$$\epsilon_0 n_i^2 r_{ijk} n_j^2 = \sum_m \alpha_{ijk}^m S_k^{m1/2} + \xi_{ijk} . \tag{7}$$

The Raman-scattering intensity of the lth oblique-phonon branch is determined from Eq. (6) in Ref. 8 and can be rewritten as follows for our two-dimensional xz plane:

$$I_{l,\varphi,k} = \left(\sum_i^{N_k} \frac{\alpha_{ik} S_{ik}^{1/2}\omega_{ik}^2}{\omega_{ik}^2 - \omega_\varphi^2} + \xi_k\right)^2 (\tilde{n}_\varphi + 1)\hbar\omega_\varphi \bigg/$$

$$\sum_i^{N_z} \frac{S_{iz}\omega_\varphi^2 \omega_{iz}^2}{\omega_{iz}^2 - \omega_\varphi^2} + \tan^2\varphi \sum_j^{N_x} \frac{S_{jx}\omega_\varphi^2 \omega_{jx}^2}{\omega_{jx}^2 - \omega_\varphi^2} . \tag{8}$$

The factors α_{ik} can be found experimentally up to a sign from the measurements of the absolute Raman-scattering intensities of the fundamental modes[21]:

$$\frac{I_{ik}(\text{TO})}{l\, d\Omega} = \frac{\omega_R^4(\omega_{ik})v}{32\pi^2\epsilon_0^2 c^4 K_k^m}\, \alpha_{ik}^2(\tilde{n}_{ik} + 1)\hbar\omega_{ik} . \tag{9}$$

$\tilde{n}$ is the thermal population factor, k denotes either the z or x axis, depending on the experimental Raman polarization filter setup (referring to the A or E_1 Raman tensor elements, respectively), v is the unit cell volume, K_k^m is the spring constant, and $\omega_R(\omega_{ik})$ is the shifted Raman frequency of the fundamental mode. The measurements of the oblique-phonon intensities provide, therefore, a new method for determining the nonlinear coefficients of the crystal.

EXPERIMENTS AND RESULTS

Several clear transparent solution grown single crystals of LiIO_3 3–10 mm on an edge were utilized during the measurements. The faces were cut and polished perpendicular to the crystallographic axes. Some crystals were grown by us from a seeded solution, others were supplied by different sources[22] in order to compare possible differences in the phonon structure due to different properties reported.[1,2] However, the spectral results from all crystals were the same.

The Raman spectra were obtained utilizing the 5145-Å line of a CRL model 52 argon-ion laser, a Spex double-monochromator model 1401, and dc recording. The Raman frequencies were measured to an absolute accuracy of about ±1 cm⁻¹.

The Raman tensor components and the experimental scattering configuration used to assign the optical phonons are shown in Figs. 2(a)–2(e). In the notation $h(ij)k$, h and k are the propagation directions of the incident and scattered light, and i and j are their polarization directions, respectively. Different geometrical configurations enable the study of the TO and LO splittings of the polar A and E_1 modes. The optical activity in LiIO_3 25 deg/mm[1] along the z axis can sometimes present a problem in identifying the selection rules. In cases similar to LiIO_3, where the total Raman information
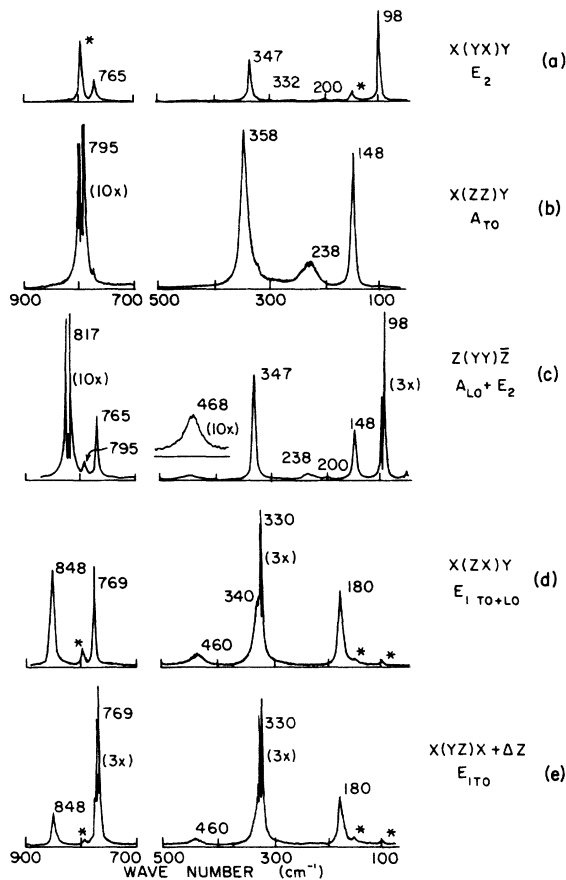
FIG. 2. Typical spectra of LiIO$_3$ for various Raman tensor components. The asterisk refers to spillover due to slight crystal misorientation.

can be obtained without the necessity of propagating the beams along the optic axis, this problem becomes minor. In certain other cases a comparison method can be used as described for the KDP spectra.[23]

The nonpolar E_2 phonons were determined by an $x(yx)y$ arrangement [Fig. 2(a)]. For the A modes the $x(zz)y$ and the $z(xx)\bar{z}$ configurations reveal separate TO and LO values [Figs. 2(b) and 2(c)]. For the E_1 mode, the TO values could be determined separately by the forward $x(yz)x + \Delta z$ configuration, whereas the $E_{1\,LO}$ values were determined by a 90° scattering $x(zx)y$ configuration which reveals simultaneously both TO and LO [Figs. 2(d) and 2(e)].

For the polar A and E_1 modes, the polarized infrared reflectivity from a single crystal was measured in the frequency range (300–900 cm^{-1}) and the unpolarized spectrum from a pressed pallet of LiIO$_3$ was measured in the region (50–300 cm^{-1}). All spectra were corrected for the 100% reflection as obtained from a gold-plated mirror. A KBr polarizer was used from 850 to 700 cm^{-1} and a polyethelene wire grid polarizer was used from 700 to

300 cm^{-1}. A homemade single-beam grating spectrometer with a Perkin Elmer model 210 monochromator enabled an accuracy of ± 2.5 cm^{-1}. The results of the infrared reflectivity for the 850–300 cm^{-1} range is shown in Fig. 3. The unpolarized reflectivity measured in the frequency range 50–300 cm^{-1} was flat at 18% and the low-frequency modes in both polarizations were out of the range of our detectibility. Combining the Raman and infrared data, the frequencies and assignments of the observed modes of LiIO$_3$ were determined and tabulated in Table I.

In order to determine the phonon contribution to the z component of the dielectric constant anomaly at high temperatures, a crystal of LiIO$_3$ was placed in a furnace with temperature control of ± 1 °C. The Raman experimental configuration of $x(zz)y$ reveals the four phonons of the A_{TO} representation. The results of three typical runs at 26, 100, and 220 °C are presented in Table II. Aside from the broadening of the lines as temperature was increased, only slight shifts in the four phonons of the A_{TO} representation were observed.

Observing the forward-scattering $x(zz)x + \Delta y$ arrangement, the polaritons of the A symmetry were studied. In measuring the polarized polaritons at low frequencies, using the forward-scattering geometries, the problem of scattered unshifted light is severe. In order to reduce the amount of scattered light entering the spectrometer, the CRL argon-ion laser was operated in single mode and an iodine filter[24] was used to absorb the 5145-Å scattered laser light before it entered the spectrometer. Excellent rejection, $\sim 10^3$, of the unshifted laser light was obtained by this method. The frequency shifts observed as a function of the energy and momentum conservation curves are shown in Fig. 4. All the TO lines of the A representation could be followed except the 238-cm^{-1} line. This line was broad and weak at right-angle scattering. Also, a strong flourescence from the iodine filter appeared in the region of this polariton. The dispersion of the upper E_1 polaritons was also followed. As their results fit the theory very well and do not contribute to the understanding of the crystal properties, so they will be omitted from discussion. (See also Refs. 25 and 26.)

To observe the mixing between the A and E_1 polar phonons, the LiIO$_3$ crystal was mounted so that it could be rotated around its y axis in a cylindrical cell filled with benzene ($n = 1.50$). Using the following right-angle scattering, $(\alpha x + \gamma z)(yy)(\gamma x - \alpha z)$, where α, γ are arbitrary ($\alpha^2 + \gamma^2 = 1$), the propagation of the momentum transfer q in the xz plane could then be monitored by simply rotating the crystal. The data presented here are more complete than the preliminary work reported earlier[6] due to the reduction in the index mismatch. This index
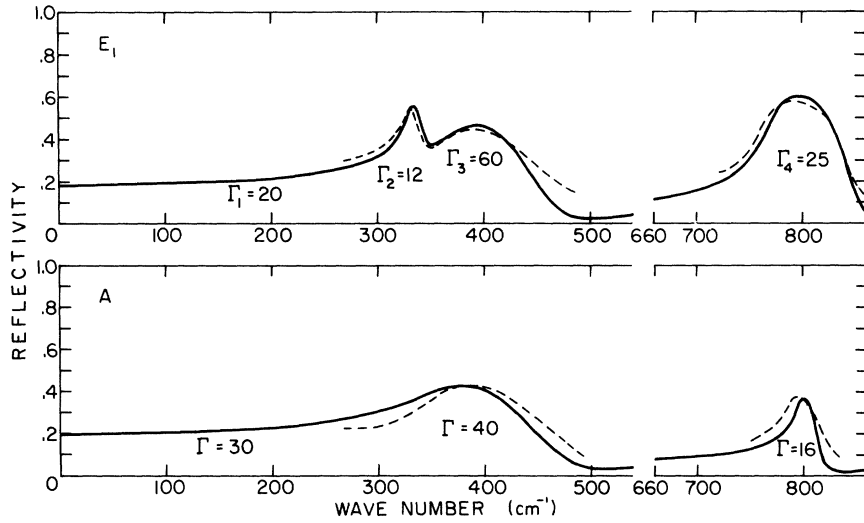
FIG. 3. Polarized infrared reflectivity spectra of LiIO$_3$. Solid curve represents experimental data. Dotted curve represents calculated reflectivity.

matching considerably reduced the amount of spurious internal reflections of the incident laser beams, which previously caused the appearance of additional lines in the spectra. The (yy) polarizability tensor component that was selected revealed the A component of the mixing. In order to cali-
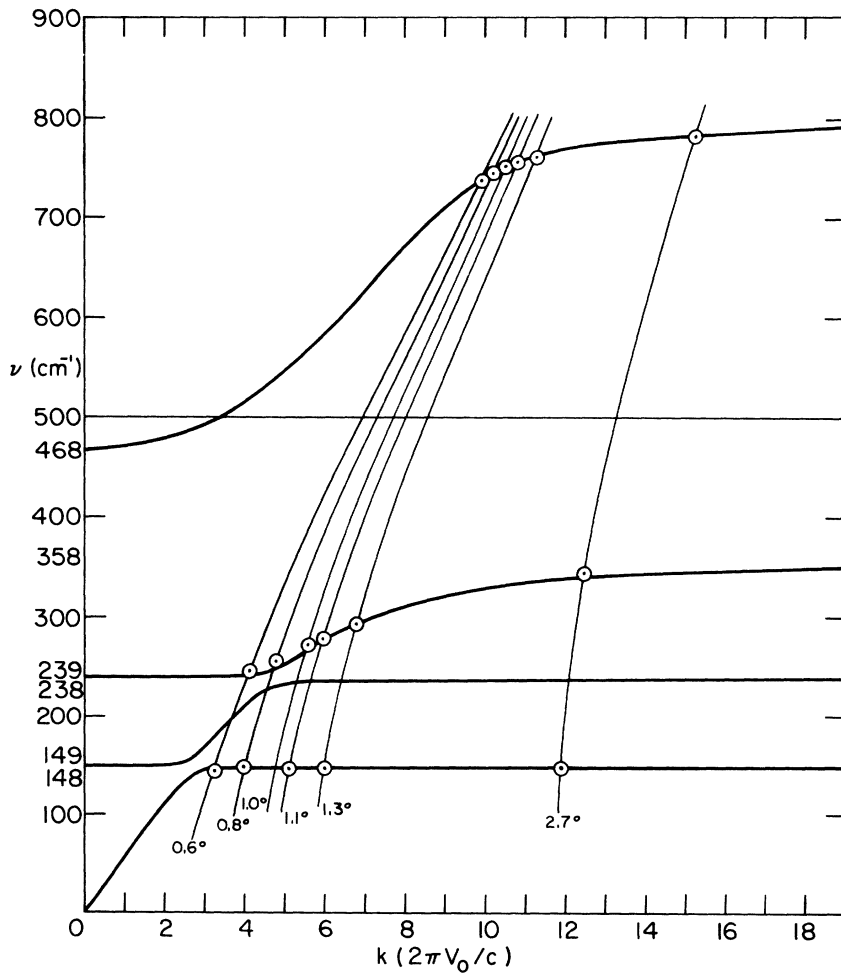

FIG. 4. Polariton dispersion curves for the A representation in LiIO$_3$ and the energy-momentum conservation curves for the scattering geometry $x(zz)x + \Delta y$.

TABLE I. Frequency assignments, dielectric transition strengths, and damping constants (Γ) for the Raman and infrared observed modes in $LiIO_3$.

Possible assignments	A(z) TO LO (cm^{-1})	Strengths	Γ	$E_1(x, y)$ TO LO (cm^{-1})	Strengths	Γ	E_2 (cm^{-1})
ν_{ext}	148	0.0826	30				98
ν_{ext}	238	0.0616	30	180	0.1026	20	200
ν_{ext}				330–340	1.672	12	332
ν_4				370–460	1.889	60	347
ν_2	358–468	2.300	40				
ν_1	795–817	0.1406	16				
ν_3				769–848	0.625	25	765

brate the intensity of the oblique phonons observed, the cross section of the mixed phonons was standardized to the 98-cm^{-1} E_2 phonon, which also appears in the yy Raman filtered spectrum without being mixed. The absolute intensity calibration [Eq. (9)] of the $I_{jk}(TO)$ was done against the cross section of the 992-cm^{-1} benzene line.[27] The observed angular dispersion and intensity of the two upper oblique-phonon branches of the $A = E_1$ mixing are shown in Figs. 5 and 6.
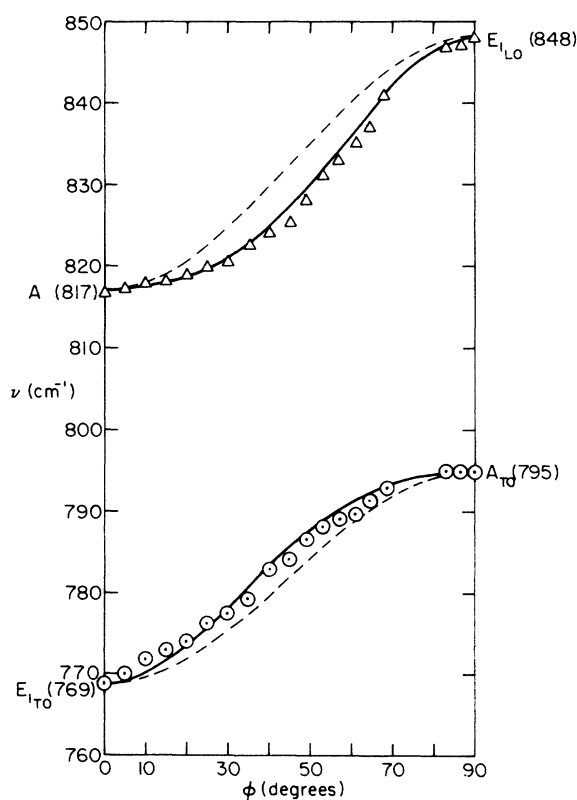

FIG. 5. Angular dispersion of the two upper $A + E_1$ symmetry oblique phonons propagating in the xz plane and observed with the (yy) Raman polarization filter.

DISCUSSION

Table I summarizes the first-order Raman-scattering data combined with the polarized infrared reflectivity results. All the modes predicted by the C_6^6 space symmetry with 2 molecules per primitive cell are accounted for. The birefringence and optical activity were minor experimental problems and were taken into account during the various measurements.

The intensity comparison between the $E_1(TO)$ + $E_1(LO)$ spectrum in Fig. 2(d) and the $E_1(TO)$ spectrum in Fig. 2(e) allows the identification of the TO and LO frequencies of three of the four modes belonging to the E_1 representation. The 370-cm^{-1} $E_1(TO)$ mode was not seen in the Raman data taken; however, its corresponding LO vibration at 460 cm^{-1} was observed. The location of the TO frequency was determined by fitting the TO-LO splittings of the E_1 modes to the polarized infrared reflectivity data (Fig. 3). The value of the missing $E_1(TO)$ mode and the damping factors were adjusted to give the best fit with the infrared data. The TO-LO splittings of the 148- and 238-cm^{-1} A-symmetry modes and the 180-cm^{-1} E_1-symmetry mode were beyond the resolution of the Raman spectrometer. However, on cooling the crystal down to liquid-

TABLE II. Frequencies of the four TO modes of the A representation in $LiIO_3$ at 27, 100, and 220 °C. The published experimental values of $\epsilon_{zz}(LST)$, $\epsilon_{zz}(MHz)$, and $\epsilon_{zz}(KHz)$ are also included.

	27 °C (cm^{-1})	100 °C (cm^{-1})	220 °C (cm^{-1})
$A(TO)$	148	146	139
$A(TO)$	238	238	238
$A(TO)$	358	358	354
$A(TO)$	795	795	795
$\epsilon_{zz}(LST)$	6.7	6.9	7.8
$\epsilon_{zz}(MHz)^a$	6.4	•••	•••
$\epsilon_{zz}(KHz)^b$	554	2900	6380

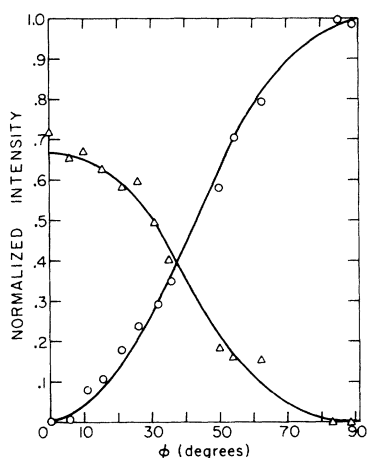[a]Reference 5.   [b]Reference 1.

FIG. 6. Raman normalized intensities of the oblique phonons of Fig. 5 (using the same notation). The intensities have been normalized to the intensity of $A_{TO} = 795$ cm^{-1} at $\varphi = 90°$.

nitrogen temperature and utilizing the $x(zx)y$ configuration, the 180-cm^{-1} mode of the E_1 symmetry changed into a doublet at 172 cm^{-1} with an LO-TO splitting of 3 cm^{-1}. The other lines of the E_1 representation were also shifted down to lower frequencies with no major spectral changes. However, measuring the A-symmetry modes at low temperatures did not reveal any detectable LO-TO separation for the two low-frequency modes. The transition strengths of the modes of the A and E_1 representations were calculated from Eq. (3) neglecting damping terms (Table I). One wave-number LO-TO splittings has been arbitrarily assumed for the 148 and 238 modes of the A symmetry and for the 180-cm^{-1} E_1-symmetry mode.

Recent Raman measurements[25] on LiIO$_3$ have revealed the strongest Raman lines in the spectra. There is an agreement up to a few wave numbers for the reported modes of the A and E_1 symmetry. However, there is a disagreement regarding the E_2-symmetry modes; the 824-cm^{-1} peak which was assigned as an E_2-symmetry mode is believed to be a spillover due to an oblique $A + E_1$ mode, which will be discussed later. All five modes of the E_2 representation have frequencies lower than 800 cm^{-1} [Fig. 2(a)].

The observed polarized infrared reflectivity data in Fig. 3 is fitted by using Eqs. (1) and (3) with the frequency values in Table I. The only parameters are the damping terms of all the modes and the frequency value of one of the E_1-symmetry TO mode, which is not seen in the Raman data. The value of this missing mode was set at 370 cm^{-1}. The dielectric transition strengths and the damping parameters used are shown in Table I. A reasonable agreement has been obtained for most of the spectra. The low-frequency lines below 300 cm^{-1}

were below the detectibility of the far-infrared spectrometer used. The constant 18% reflectivity at 50 cm^{-1} results in an average dielectric constant [Eq. (1)] of about 7 for LiIO$_3$.

The dielectric constants ϵ_{xx} and ϵ_{zz}, which have been calculated from the generalized LST relation (4), are given in Table III. Good agreement has been obtained with the values reported by Warner et al.[5] in the MHz frequency range, yet the lower value obtained for ϵ_{zz} is significant. There is, therefore, no phonon contribution to the high dielectric constant reported at very low frequencies.[1] Most probably this high dielectric response at low frequencies is caused by a macroscopic mechanism in the crystal. Possible low-frequency wall domain response[28] or collective long-range dipole fluctuations are expected in LiIO$_3$. Efforts are now in progress to detect them experimentally.

Heating the crystal up to 220 °C has not revealed an appreciable change in the frequencies of any of the modes in the A(TO) configuration (Table II). The resulting ϵ(LST) values for several temperatures, assuming the LO frequencies to remain unchanged, are also shown in Table II. No softening of any of the A-symmetry modes was observed toward the phase transition (256 °C). There is a very slight temperature variation of the phonon-frequency dielectric constant, which can not explain the experimental increase of the low-frequency dielectric constant observed by Nash et al.[1] We have to conclude that the mechanism of the phase transition in LiIO$_3$ is not similar to that of the softening of an optical phonon at the origin of the Brillouin zone observed in many displacive ferroelectric crystals.[14,15] No clue to the phase-transition mechanism at 256 °C has been obtained, but from the dramatic increase in the low-frequency dielectric constant,[2] a macroscopic low-frequency instability can be speculated.

Another estimation for the phonon contribution to the dielectric constant ϵ_{zz} is the measurement of the lowest-A polariton dispersion.[18] The slope of this polariton at $k = 0$ is proportional to $\epsilon_{zz}^{-1/2}$(LST). Using Eq. (5) while neglecting damping, the theoretical dispersion for all four modes of the A sym-

TABLE III. Comparison of the dielectric constant for A E_1 representations of LiIO$_3$.

	This work		Warner et al.[a,b]		Nash et al.[c]
	$\sum S_i$	ϵ (LST)	ϵ_∞	ϵ (MHz)	ϵ (KHz)
$A(z)$	3.1	6.1	3.06	6.4	554
$E_1(x, y)$	3.1	6.7	3.61	8.2	65

[a]Reference 5.
[b]Lately some larger values were reported [ϵ_{zz}^T(>MHz) = 9, ϵ_{xx}^T(>MHz) = 13] by G. Arlt et al. [Phys. Status Solidi 3(a), K243 (1970)].
[c]Reference 1.

metry are computer plotted in Fig. 4. The values of the TO and LO frequencies in Table I are used. The upper polariton branch is not strongly dependent on ϵ_{zz} (LST) and has therefore been used to position the energy and momentum conservation curves for the $x(zz)x + \Delta y$ experimental arrangement. The scattering angle is thus determined to within $\pm 0.1°$. Previous measurements[25] reported the lowest value of this upper branch polariton to be 747 cm^{-1}, whereas the present results extend to 737 cm^{-1} at $0.6°$. Also, the 358-cm^{-1} TO line is observed to shift down to 247 cm^{-1} at that low scattering angle. However, the lowest 149-cm^{-1} polariton has shifted only to 145 cm^{-1} at $0.6°$ scattering angle. The theoretical curves are in good agreement with the experimental results for the low polariton branches observed. The low value for the ϵ_{zz}(LST) calculated previously from the phonon contribution is again verified. From the lowest obtained frequency point of the A characterized polariton, ϵ_{zz}(LST) can be estimated to be ~ 10.

In a preliminary publication[6] the intensity and angular dispersion of the upper two oblique-phonon branches were reported for LiIO$_3$. This mixture of the modes of the A and E_1 symmetries was observed while monitoring the momentum transfer of the Raman scattering at oblique angles in the xz plane. At that time an attempt was made to fit the angular-dispersion data with the prediction of one of Loudon's approximations,[29] namely, assuming the

long-range electrostatic field dominance over anisotropy, even when the inequality of their frequency splitting is obviously not satisfied. The intensity seemed at first approximation to follow a pure sine-cosine function. Refining the experimental procedure by using a larger crystal and index matching provided more precise and detailed results for these upper $A + E_1$ oblique phonons.[7] Also during this time a more general theory was developed,[8] which results in very simple expressions for the oblique-phonon angular dispersion and intensity behavior [Eqs. (6) and (8)]. This theory is not practically limited as before to the extreme conditions, namely either of long-range electric field or anisotropic dominance, and is applicable to multi-atomic-unit-cells of crystals belonging to orthorhombic or higher symmetries. A paper published lately[30] demonstrated the complication of the old approach when applying to an orthorhombic crystal, even with 2 atoms per unit cell.

Owing to the frequency isolation of the two interacting modes at the frequency range (769–848 cm^{-1}) discussed in this experiment, Eqs. (6) and (8) can be rewritten for only the two upper A and E_1 symmetry modes as follows:

$$\tan^2\varphi_j = -\frac{\epsilon_{\infty A}(\omega_{TO\,E_1}^2 - \omega_{\varphi j}^2)(\omega_{LO\,A}^2 - \omega_{\varphi j}^2)}{\epsilon_{\infty E_1}(\omega_{TO\,A}^2 - \omega_{\varphi j}^2)(\omega_{LO\,E_1}^2 - \omega_{\varphi j})} \quad (10)$$

and

$$\frac{I_{j\varphi j z}}{I_{TO\,A}} = \omega_{R,\varphi j}^4 \left[1 + \frac{\xi_{13}}{\alpha_{13}}\left(\frac{\omega_{TO\,A}^2 - \omega_{\varphi j}^2}{S_A^{1/2}\omega_{TO\,A}^2}\right)\right]^2 \frac{\omega_{\varphi j}}{\omega_{TO\,A}} \frac{1 - e^{-\hbar\omega_{TO\,A}/kT}}{1 - \exp(-\hbar\omega_{\varphi j}/kT)} \Big/$$

$$\omega_{R,TO}^4 \left[\frac{\omega_{\varphi j}^2}{\omega_{TO\,A}^2} - \frac{\epsilon_{\infty A}S_{E_1}\omega_{\varphi j}^2\,\omega_{TO\,E_1}^2(\omega_{LO\,A}^2 - \omega_{\varphi j}^2)(\omega_{TO\,A}^2 - \omega_{\varphi j}^2)}{\epsilon_{\infty E_1}S_A\,\omega_{TO\,A}^4(\omega_{LO\,E_1}^2 - \omega_{\varphi j}^2)(\omega_{TO\,E_1}^2 - \omega_{\varphi j}^2)}\right] \quad , \quad (11)$$

where Eq. (11) has been normalized with the intensity of the $A_{TO} = 795$ cm^{-1} fundamental mode at $\varphi = 90°$.

The experimental data of the angular dispersion in LiIO$_3$, obtained for an oblique phonon propagating in the xz plane and with the (yy) Raman polarization filter, is shown in Fig. 5. The solid curve represents the theoretical predictions of Eq. (10), applied to the upper phonons of A and E_1 symmetries and utilizing the TO and LO frequencies in Table I. Excellent agreement with Eq. (10) was obtained all along the dispersion range. The dashed line is a replot of Loudon's approximated equations used earlier,[6] under the long-range electric-field-dominance assumption and the same endpoints of Table I. The dashed lines in Fig. 5 are more separated indicating that excess interaction was provided to the system through the previous approximation.

It is believed, therefore, that the set of equations

TABLE IV. Linear electro-optic term r_{13} and the SHG d_{13} in LiIO$_3$ as determined experimentally by several methods.

	10^{-12} r_{13}	10^{-22} d_{13}	$\lambda(\mu)$	Method
Present work	$\pm 5.8 \pm 1.2$	0.90 ± 0.18	0.5145	Raman oblique phonons
Nash et al. (Ref. 1)	4.1 ± 0.6		0.6328	Hetrodyne
		0.63 ± 0.20^a	1.06	SHG
Jerphagnon (Ref. 9)		0.68 ± 0.18^a	1.06	Maker fringe
Nath et al. (Ref. 29)		$0.68^{a,b}$	0.6943	SHG
Campillo and Tang (Ref. 30)		0.69 ± 0.18^a	0.5145	Spontaneous parametric scattering

^{a}These absolute values are based on the reported ratio (Ref. 31) d_{13}(LiNbO$_3$)$/d_{36}$(KDP) $= 10.1 \pm 16\%$ and the value d_{13}(LiNbO$_3$) $= 0.58 \times 10^{-22}$ (Ref. 32).

^{b}A higher value for the SHG of LiIO$_3$ was reported by Nath et al.[29] but was corrected lately to the given value.

developed for two- or three-dimensional dielectric spaces would be utilized to study more complicated multi-oblique-phonon crystals. When such oblique phonons are confined to propagate in a plane, a gap-frequency-type picture results from the explicit Eq. (6). The shape of the angular-dispersion curves will then be predicted and will depend only on the relative positioning of the pure TO and LO

frequencies of all the modes involved.

The ratio $|R| = |\xi_{13}/\alpha_{13}|$ is the only parameter to be fitted [Eq. (11)] with the experimental intensity data along the angular-dispersion range. This ratio can also be determined from the endpoints, namely, in our case from the ratio of intensities $I_{LO\,A}/I_{TO\,A}$ of the LO and TO values of the upper A-symmetry mode:

$$|R| = \left| \frac{\xi_{13}}{\alpha_{13}} \right| = \epsilon_{\infty_\ell} S_A^{-1/2} \left[1 \pm \left(\frac{I_{LO\,A}}{I_{TO\,A}} \frac{\omega_{LO\,A}(1 - e^{-\hbar\omega_{LO\,A}/kT})}{\omega_{TO\,A}(1 - \exp(-\hbar\omega_{TO\,A}/kT))} \right)^{1/2} \right] . \quad (12)$$

Equation (12) applies under the same assumption of mixing only between the two upper branches, as in Eq. (10). The linear electro-optic coefficient is then determined from

$$r_{13} = \left[\left(\frac{32\pi^2\epsilon_0 c^4 S_A}{n^8 \hbar\omega_m \omega_s^4 (n_0^m + 1)} \right) \frac{I_{TO\,A}}{I\,d\Omega} \right]^{1/2} \left(1 + \frac{R}{S_A^{1/2}} \right) \quad (13)$$

and the SHG term is

$$d_{13} = - \frac{\epsilon_0 \epsilon_\infty^2 r_{13}}{4(1 + S_A^{1/2})/R} . \quad (14)$$

The intensity ratio at $\varphi = 0$ (Fig. 6) of $I_{LO\,A}/I_{TO\,A}$ = 0.67 results in $R = 1.23$ or 13.3 due to the ambiguity sign in Eq. (12). This sign ambiguity is quickly resolved when Eq. (11) is plotted using these two values of R for ξ_{13}/α_{13} and comparing the resulting curves with the experimental results. The solid line in Fig. 6 represents the theoretical intensity of Eq. (11) using $R = 1.23$. The values of r_{13} and d_{13} in LiIO$_3$ are compared in Table IV with other published values. The experimental error was estimated as $\pm 15\%$, in which the largest source of experimental error is still due to $\pm 10\%$ error in the determination of the benzene absolute cross section. [27]

The values obtained for r_{13}(LiIO$_3$) and d_{13}(LiIO$_3$) in the present work are slightly higher than those reported by other methods, but they are still within the experimental error. In comparison with Raman measurements of the nonlinear coefficients in other piezoelectric crystals, [21] several differences are noticed: Kaminow and Johnston[21] reported for LiNbO$_3$ that the "softest" modes, which contribute mostly to the static dielectric constant, contribute also the largest amount to the electro-optic behavior. In our case the upper A mode used in determining the

linear electro-optic coefficient r_{13} of LiIO$_3$ does not make the largest contribution to the static dielectric constant. The contribution of the next-lower mode of the A symmetry will have little affect on the r_{13} calculated due to their low scattering efficiency with the (yy) Raman polarization filter. The other two lower modes of the A symmetry have small dielectric transition strengths, which will further reduce their contributions. Kaminow and Johnston[21] also observed that in LiNbO$_3$ the pure electronic contribution is less than 10% of the lattice contribution to r_{ijk}. In LiIO$_3$ within the approximations used the pure electronic contribution is about 75% of the lattice contribution.

This method to measure the electro-optic coefficients is applicable to polar crystals of orthorhombic symmetry or higher in which the oblique-phonon intensities can be measured throughout the angular-dispersion range. Generally, the value of d_{ijk} can be determined from any separated branch. However, the value of r_{ijk} can be determined only if all the modes are considered. The sign of d_{ijk} relative to r_{ijk} can usually be determined by best fitting to the experimental data. The present method, which fits the total angular-dispersion range, provides a more reliable method to determine $|r_{ijk}|$ and $|d_{ijk}|$ and their relative sign than the Raman cross-section measurements of just the LO and TO endpoints used heretofore.

ACKNOWLEDGMENTS

[1] F. R. Nash, J. G. Bergman, G. D. Boyd, and E. H. Turner, J. Appl. Phys. 40, 5201 (1969).

[2] G. Nath and S. Haussuhl, Appl. Phys. Letters 14, 154 (1969).

[3] A. Rosenzweig and B. Morosin, Acta Cryst. 20, 758 (1966).

[4] W. H. Zachariasen and F. A. Barta, Phys. Rev. 37, 1626 (1931).

[5] A. W. Warner, J. G. Bergman, D. A. Pinnow, and

G. R. Crane, J. Acoust. Soc. Am. **47**, 791 (1970).

[6]W. Otaguro, C. A. Arguello, and S. P. S. Porto, Phys. Rev. B **1**, 2818 (1970).

[7]W. S. Otaguro, E. Wiener-Avnear, and S. P. S. Porto, Appl. Phys. Letters (to be published).

[8]C. M. Hartwig, E. Wiener-Avnear, J. Smit, and S. P. S. Porto, Phys. Rev. B **3**, 2078 (1971).

[9]J. Jerphagnon, Appl. Phys. Letters **16**, 298 (1970).

[10]G. Nath, H. Mehmanesch, and M. Gsänger, Appl. Phys. Letters **17**, 286 (1970) (previous report with a higher value for the SHG, Ref. 2).

[11]A. J. Campillo and C. L. Tang, Appl. Phys. Letters **16**, 242 (1970); **16**, 537(E) (1970).

[12]W. E. Dasent and T. C. Waddington, J. Chem. Soc. **XX**, 2429 (1960).

[13]C. Haas and D. F. Hornig, J. Chem. Phys. **26**, 707 (1957); E. Burstein, in *Dynamical Processes in Solid State Optics*, edited by R. Kubo and H. Kamimura (Benjamin, New York, 1967), pp. 1–33.

[14]W. Cochran, Advan. Phys. **9**, 387 (1960).

[15]M. Di Domenico, Jr., S. H. Wemple, and S. P. S. Porto, Phys. Rev. **174**, 522 (1968).

[16]C. H. Henry and J. J. Hopfield, Phys. Rev. Letters **15**, 964 (1965).

[17]S. P. S. Porto, B. Tell, and T. C. Damen, Phys. Rev. Letters **16**, 450 (1966).

[18]E. Burstein, S. Ushioda, A. Pinczuk, and J. Scott, in *Proceedings of the International Conference on Light Scattering Spectra in Solids, New York University, 1968*, edited by G. B. Wright (Springer-Verlag, New York, 1969).

[19]C. A. Arguello, D. L. Rousseau, and S. P. S. Porto, Phys. Rev. **181**, 1351 (1969).

[20]I. P. Kaminow, in *Ferroelectricity: Proceedings of the Symposium on Ferroelectricity, General Motors Research Laboratories, Warren, Mich.*, 1966 (Elsevier, Houston, Tex., 1966).

[21]I. P. Kaminow and W. D. Johnston, Jr., Phys. Rev. **160**, 519 (1967); **178**, 1528(E) (1969); W. D. Johnston Jr. and I. P. Kaminow, *ibid.* **188**, 1209 (1969).

[22]Crystals were kindly sent to us by G. Nath, Physik-Department der Technischen Hochschule, München, München, Germany, and J. G. Bergman, Bell Telephone Laboratories, Murray Hill, N. J.

[23]E. Wiener-Avnear and S. P. S. Porto (unpublished).

[24]Lewis Fraas, thesis (University of Southern California, 1971) (unpublished).

[25]R. Claus, H. W. Schrotter, H. H. Hacher, and S. Haussuhl, Z. Naturforsch. **24a**, 1733 (1969); R. Claus, *ibid.* **25a**, 306 (1970).

[26]C. K. Asawa and M. K. Barnoski, Phys. Rev. B **3**, 2682 (1971).

[27]J. G. Skinner and W. G. Nilsen, J. Opt. Soc. Am. **58**, 113 (1968); P. E. Schoen, H. Z. Cummins, and R. L. Reese, Bull. Am. Phys. Soc. **16**, 29 (1971).

[28]F. Jona and G. Shirane, *Ferroelectric Crystals* (Pergamon, New York, 1962).

[29]R. Loudon, Advan. Phys. **13**, 423 (1966).

[30]C. K. Asawa, Phys. Rev. B **2**, 2068 (1970).

[31]J. E. Bjorkholm, J. Quantum Electron. **QE4**, 970 (1968).

[32]S. E. Harris, Chromatix Tech. Letters **1**, 1 (1969).

Lattice Dynamics of KN₃

K. R. Rao,* S. F. Trevino,[†] and H. Prask[†]
Explosives Laboratory, Feltman Research Laboratory, Picatinny Arsenal, Dover, New Jersey 07801

and

R. D. Mical[‡]
Boston College, Chestnut Hill, Massachusetts 02167
(Received 21 June 1971)

In this paper we report the measurement of several acoustic-phonon modes in KN₃. Results for the longitudinal and doubly degenerate transverse modes along the [00μ] directions and the longitudinal and one transverse mode (polarized along the c axis) propagating along the [μμ0] direction are presented. The measurements are compared with a calculation based on a rigid-ion model. The model includes point charges at the position of the cation and at the center of the anion. The short-range repulsive interaction is a modified Huggins-Mayer potential with the cation treated as spherical and the anion as an ellipsoid of revolution. Adequate agreement is obtained with the present neutron-scattering measurement and with recent infrared and Raman results.

I. INTRODUCTION

Metal azide salts form an interesting family of materials which exhibit a broad range of crystal stabilities. The structure of most of the light-metal azides and several of the heavy-metal azides is known. In the light-metal azides, the azide ion is linear and symmetric, whereas in the heavy-metal salts, which are considerably less stable, there exist asymmetric and nonlinear azide ions. This has lead to the speculation that the interactions of the metal and azide ions change qualitatively between the light- and heavy-metal compounds. This difference in the type of bonding could be significant in explaining the markedly different stabilities. An investigation of the lattice dynamics of these crystals would seem a fruitful study for the purpose of testing these ideas.